Chapter 2
Introduction to Quantum Transport in the Time Domain

The study of quantum transport is the study of the flow of electrons through small electronic circuits, typically of a few microns (μm) in extent and cooled to cryogenic temperatures <1 K. At such small length scales, and at such low temperatures, the electrons behave according to the laws of quantum mechanics, which gives rise to behaviour that is *qualitatively different* compared to the classical behaviour, due to the fact that the electrons now behave as waves. The field of quantum transport is now entering a new era as it becomes possible to modify these circuit devices on shorter and shorter time scales. In practice this could involve applying a quickly-changing bias voltage across the device or rapidly charging and discharging a nearby capacitor. Operating on ever shorter timescales allows us to access qualitatively different regimes of operation for these devices, where we can start to probe the *internal dynamics* far beyond the adiabatic limit.

In this thesis we are concerned with the theoretical and numerical techniques required for treating this so-called "time-resolved quantum transport". This chapter contains a general introduction to the field of quantum transport, discussing the relevant length and time scales, before moving on to the recent experimental progress that serves as a motivation for studying the emerging sub-field of time-resolved transport. Finally, we discuss existing theoretical and numerical techniques for treating problems in this field.

2.1 Mesoscopic Quantum Electronics

Let us begin by getting a general feel for the sort of devices and length scales with which we will be concerned in this thesis. In general we will be studying the *coherent* transport of electrons, that is, where their quantum-mechanical wave-like nature is exhibited; this is also referred to as *quantum* transport. This already puts an upper bound on the size of circuit that we wish to consider. If we want to be able to observe

J. Weston, *Numerical Methods for Time-Resolved Quantum Nanoelectronics*,
Springer Theses, DOI 10.1007/978-3-319-63691-7_2

quantum effects (notably interference), the phase of the electronic wavefunction must remain well-defined across the system. At distances greater than L_φ—the *coherence length*—the electronic wavefunction will lose its well-defined phase; the characteristic quantum interference will tend to be washed out. The physical origin of the finite coherence length is related to interactions of the electrons with other degrees of freedom in the material (e.g. lattice vibrations, impurities with some internal degrees of freedom, or electron-electron interactions) [1, 2]. Naturally, then, the coherence length will strongly depend on temperature; we will normally have to descend to cryogenic temperatures (<1 K) in order to "freeze out" the non-electronic degrees of freedom that will give rise to decoherence. At these temperatures coherence lengths of the order of tens of μm have been measured experimentally in certain semiconductor heterostructures [3]. In this thesis we will not be concerned with the process of decoherence per se, however we will always have to remember to place ourselves in an appropriate parameter regime (with respect to system size and temperature) so that decoherence is not an issue.

We will also impose a lower-bound on the length scales of interest to us; we do not want to describe details on the scale of single atoms. While devices such as molecular junctions—where a molecule is suspended between large metallic contacts—can, in principle, be described by the techniques that we will present [4], this is not our domain of interest. We will mostly be interested in cases where the electrons in a material "see" the underlying ionic lattice as a continuum, and the specific material properties enter only in the effective mass of the electrons [1]. This is valid when the Fermi wavelength of the electrons is large compared to the inter-atomic distance. This range of distances, of the order of a few μm but larger than atomic distances, is referred to as the "mesoscopic" scale.

Another key feature of electronics at the mesoscopic scale is that devices are usually constructed so that the electronic motion is restricted in one or more spatial dimensions. For the electrons, the circuit is effectively two or one dimensional, even though the actual device obviously exists in three dimensions. The archetypal mesoscopic system is the two-dimensional electron gas (2DEG) that forms at the interface between layers of aluminium gallium arsenide and gallium arsenide; a sketch is shown in Fig. 2.1a. Figure 2.1a also shows a simplified sketch of the valence/conductance bands at the interface of such a heterostructure; we see that the charge transfer that equalises the Fermi level on either side of the interface induces an electric field that confines electrons close to the interface. The electronic confinement along the z direction leads to quantization of the z component of the quasi momentum p_z, although the electrons are still quasi-free in the $x - y$ plane parallel to the interface. This quantization effectively "freezes out" the z degree of freedom, as long as any perturbations made to the 2DEG are small compared to the energy required to transition to a state with different p_z. Figure 2.1b shows a scanning electron microscope image of a mesoscopic circuit constructed from such a heterostructure. The 2DEG is in a plane parallel to the image, embedded $\sim$100 nm below the surface. The lighter grey rectangles are made of metal deposited on top of the heterostructure, and are referred to as "gates". As the gates are separated from the 2DEG by a layer of semiconductor (which is insulating) no electrons flow between

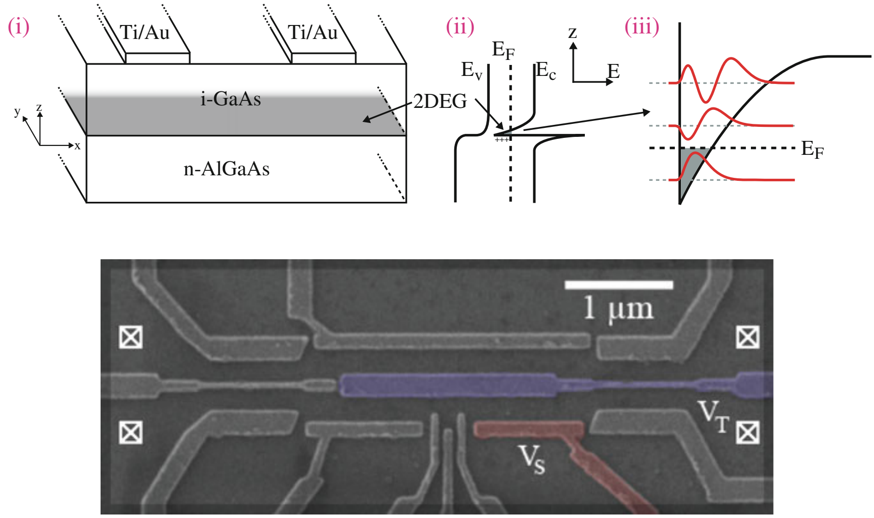

Fig. 2.1 Illustrations of a 2DEG; a conceptual picture, and the experimental reality. **a** (i) Sketch of an AlGaAs/GaAs heterostructure with a 2DEG at the interface and metallic Ti/Au gates deposited on the surface. (ii) Sketch of the conduction (E_c) and valence (E_v) bands in the vicinity of the interface. The "+" symbols show the positively charged donors and the 2DEG is indicated in grey. (iii) A sketch of the quantised modes in the z direction; in this example only the lowest mode is populated as the others are above the Fermi energy (E_F). **b** Scanning electron microscope image of a flying qubit interferometer in an AlGaAs/GaAs 2DEG. The 2DEG is in a plane parallel to the page and roughly 100 nm below it. The *lighter grey regions* are metallic gates deposited on the surface of the heterostructure. Reprinted with permission from Ref. [6], copyright 2015 by the American Physical Society

the gates and the 2DEG. If a voltage is applied to a gate, however, the electrons in the 2DEG will feel the electric field produced; this can be used to confine the electrons within subregions of the 2DEG. The white squares in Fig. 2.1b indicate where electrons will be able to flow in/out of the 2DEG through ohmic contacts [5] into metallic *leads* (we will also refer to these as *electrodes* or *contacts*). These leads interface the quantum circuit with the macroscopic world, which consists of the measurement apparatus, voltage sources, radio-frequency transmission lines etc.

In this thesis we will be developing and applying numerical techniques to simulate the behaviour of these sorts of mesoscopic devices when their controlling parameters (such as the gate or bias voltages discussed above) are modified quickly enough to probe the internal dynamics of the device. Concretely this means varying the control parameters quickly compared to the time it takes an electron to traverse the device. In the 2DEGs discussed above the electrons at the Fermi level typically travel at speeds of 10^4–10^5 m s^{-1} [7], which means that the control parameters need to vary at frequencies in the range of tens of GHz, when the device is a few μm in length. In addition, we also need to excite electrons at energies higher than the thermal background if we hope to measure anything. This presents a less stringent constraint, however, as quantum transport experiments are typically carried out at temperatures $\ll 1\,\mathrm{K}$, which corresponds to frequencies less than $20\,\mathrm{GH}_Z$. We refer to quantum transport in the presence of time-varying device parameters as time-*dependent* transport, and reserve the more specific term time-*resolved* transport to refer to the case where the internal device dynamics are probed.

2.2 Experiments in the Time Domain

One of the first examples of time-*dependent* quantum transport being studied in the laboratory was the measurement of photo-assisted tunnelling by Tien and Gordon [8], where the presence of an a.c. bias voltage affects the d.c. current flowing through a device. This was followed, at around the same time, by the discovery of the a.c. Josephson effect [9, 10], where a d.c. bias voltage causes an a.c. output current in a superconducting junction. Over the years several other novel effects at finite frequency were discovered, such as charge pumping [11, 12] (where a purely a.c. voltage with no d.c. component can induce a d.c. current).

The recent move towards time-*resolved* transport has been motivated by the desire to build coherent sources of single electrons. To see why these two ideas are linked, let's consider the application of a finite, static bias to an electrode of a quantum circuit. This can be seen as producing a continuous stream of electrons that flow from the biased electrode to be collected by the other (grounded) electrodes. If we now apply the bias only during a finite time interval, we will clearly only transfer a finite number of charges. As we reduce the time over which we apply the bias we will eventually arrive at the point where the bias "pulse" is so brief that only a single charge is transferred. We refer to such weak/brief bias pulses as being "in the quantum regime" when they only excite one or a few charges, i.e.

$$n = \frac{e}{h} \int V(t) \mathrm{d}t, \tag{2.1}$$

where n is a small integer. Although in practice the generation of coherent single electrons is more complicated than this naïve picture, it nevertheless motivates why a time-*resolved* description will be necessary.

The first single-electron sources were realised using a different paradigm to the one outlined above. Instead of applying a bias voltage to inject electrons from an electrode into the quantum device, gates were used confine electrons in a region of a 2DEG with size comparable to the Fermi wavelength [13–15]. As a result the electrons in this so-called "quantum dot" have their energy quantised; A gate applied

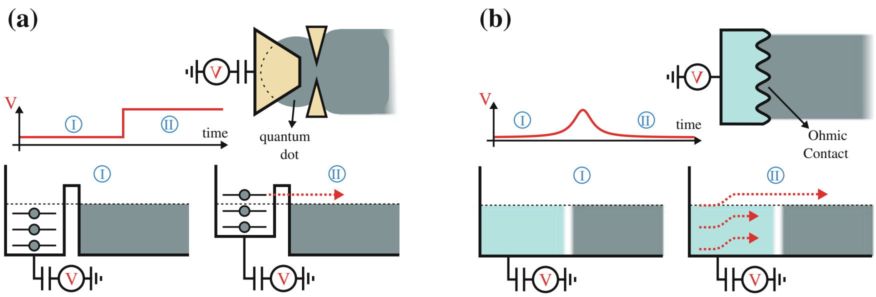

Fig. 2.2 Two techniques for producing coherent single-electron excitations in quantum circuits, that were both recently realised experimentally. **a** Single-electron source using a quantum dot in a 2DEG. The schematic (*top-right*) shows how the gates (*light grey*) constrict the 2DEG (*dark grey*) to form a quantum dot with discrete energy levels. The voltage V applied to the top-gate shifts the levels of the dot to bring a single electron above the Fermi energy in the rest of the 2DEG; the electron tunnels through the barrier and escapes. **b** Single-electron source using a lorentzian pulse applied to an ohmic contact. The schematic (*top-right*) shows the ohmic contact (*light grey*) via which charges can be *injected* from the lead into the attached to the 2DEG (*dark grey*). The bias voltage pulse V excites the Fermi sea of the lead; the specific form of the pulse ensures that when $(e/h)\int V(t)\mathrm{d}t = 1$ the net result is that only a *single electron* is excited, and the Fermi sea remains undisturbed (see main text)

to the top of the confined region is used to shift the energy levels of the underlying quantum dot so that a single electron is brought above the Fermi energy of the surrounding 2DEG. The electron can then tunnel through the confining potential and propagate into the rest of the 2DEG, as illustrated in Fig. 2.2a. This setup can produce single electrons with well-defined energy, but poorly defined release time (due to the Heisenberg uncertainty relation $\Delta E \Delta t > \hbar/2$). Such single-electron sources were used to probe the electronic wave-particle duality in a Hanbury-Brown-Twiss (HBT) setup [16]. Additionally the fermionic nature of electrons was visualised through anti-bunching behaviour in a Hong-Ou-Mandel (HOM) setup [17].

This last experiment highlights the importance of the *fermionic* nature of the electrons when treating such mesoscopic devices. As this point will be important for our discussion of theoretical methods for time-resolved transport, we shall look at the experiment of Ref. [17] a bit more closely. Figure 2.3a shows an annotated electron microscope image of the experimental setup. A 2DEG (dark grey) is attached to several electrodes (white boxes), and gates (light grey fingers) constrict the 2DEG at the location marked "beamsplitter", which will cause the electronic wavefunction to be partially reflected. The gates marked "source 1" and "source 2" are cover the quantum dots, which host electrons that can be excited into the surrounding 2DEG by raising the gate voltage (i.e. the single-electron sources originally realised in Ref. [13]). A perpendicular magnetic field is applied to the device, which causes the electrons to propagate in unidirectional edge channels in the 2DEG[1] (shown as paths with arrows in Fig. 2.3a). The idea of the experiment is to send voltage pulses onto the

[1]This is the quantum Hall effect, which will be briefly discussed in Sect. 4.3.2.

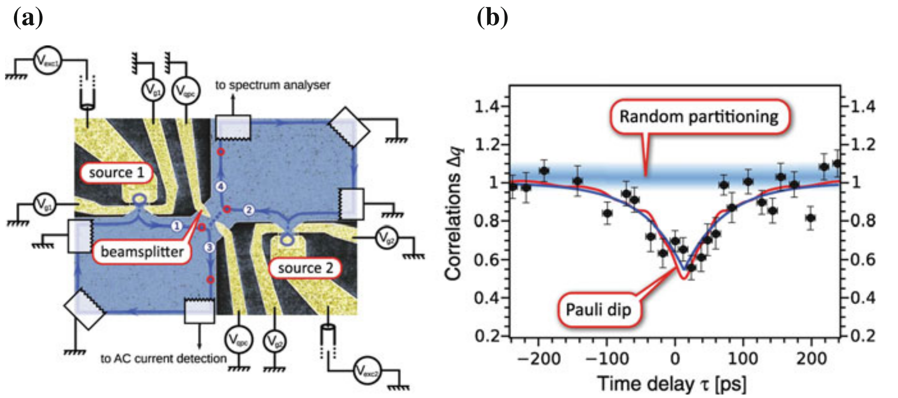

Fig. 2.3 Experimental results from Ref. [17], showing how the fluctuations in the electric current are affected when two identical electron wavepackets are incident on opposite sides of an electronic beam splitter. When the delay between the arrival of the wavepackets is small, there is a dip in the current fluctuations due to the Pauli principle. Both subfigures are from Ref. [17] and reprinted with permission from AAAS. **a** Annotated electron microscope image of the experimental setup. Metallic gates (*light grey*) are capacitively coupled to an embedded 2DEG (*dark grey*). Ohmic contacts (*white boxes*) measure the output current. **b** Excess noise in the number of transmitted particles as a function of the delay between the emission of single electrons from source 1 and source 2

gates "source 1" and "source 2" with a slight delay relative to one another. This will mean that two electrons will be excited above the Fermi sea, one at source 1 and the other at source 2, which will begin propagating towards the beamsplitter (along paths 1 and 2 in Fig. 2.3a). As the voltage pulse is sent to source 2 with a delay with respect to the voltage pulse sent to source 1, the electrons from the two sources will arrive at the beamsplitter with a corresponding delay. In the case where the electrons arrive at the beam splitter at the same time they must exit along *different* paths (3 or 4); if they exit along the same path they would be in identical states, which is disallowed due to the Pauli principle. There are two possibilities: both electrons are transmitted, or both particles are reflected, in either case each of the contacts on the paths 3 and 4 will receive *exactly* 1 *electron*. If the electrons arrive slightly delayed then it is possible that they both exit the beamsplitter along the same path, as they will not be perfectly overlapping (and hence not in the same state) in this case. Unfortunately it is not yet experimentally possible to have one-shot detection of ballistically propagating single electrons in condensed matter. Instead, experimentalists will typically generate *many* single-electron excitations one after the other and then measure the *average* current, as well as its noise properties.[2] In the HOM setup the Pauli principle should then manifest itself in a reduction of the current noise when there is no delay between the arrival of the electrons; this is shown in Fig. 2.3b.

[2]The time delay between the subsequent single-electron excitations should, therefore, be much greater than the time it takes for an electron to traverse the device.

Later, another method of producing coherent single-electron excitations was demonstrated [18, 19]. Here, instead of initially confining electrons in a quantum dot, a Lorentzian-shaped voltage pulse applied to an electrode coupled to the 2DEG via an ohmic contact *injects* a single-electron excitation from the electrode into the 2DEG. Figure 2.2b shows an illustration of this approach, which can be compared to the quantum dot approach discussed previously. These experiments were motivated by the seminal work of Levitov [20, 21], who showed that the *shape* (or equivalently, the harmonic content) of the voltage pulse is of tantamount importance in the generation of coherent single-electron excitations. Applying an arbitrary voltage pulse will, in general, perturb the Fermi sea and produce excitations above the Fermi energy (electron-like excitations) as well as below (hole-like excitations), which will both propagate into the device. Levitov showed that when a *Lorenzian* pulse is used only electron-like excitations above the Fermi energy will propagate into the device.[3] Such a Lorentzian pulse $V(t) = V_p/[(t - t_0)^2 + 1]$ can excite a *single electron*, above an undisturbed Fermi sea, when $(e/h) \int V(t)\mathrm{d}t = 1$. Such excitations are referred to as *Levitons*. Owing to the continuum of energy states in the electrode (as opposed to the discrete levels of the quantum dot), the excitation is poorly resolved in energy but *well* resolved in time. We should emphasise that this is a *completely* different paradigm for generating single-charge excitations than the quantum dot approach of Ref. [13]. While the approach using quantum dots can be understood as tuning the levels in the dot to put a single level (and hence single electron) above the surrounding Fermi sea, the Leviton is instead a *collective excitation* of the Fermi sea itself. That such a collective excitation consists, in the end, of an unperturbed Fermi sea with unentangled, purely electron-like excitations on top is far from obvious [21].

After their experimental discovery, Levitons were then used in HBT and HOM setups [19] analogous to those of Refs. [16, 17]. Figure 2.4a shows an artist's impression of the HOM experimental setup, and the results of current noise measurements are shown in Fig. 2.4b. We clearly see that the noise drops to zero when the two Levitons arrive at the beamsplitter with no time delay, which is due to the Pauli principle, as discussed previously. Even more recent experiments used shot noise measurements to directly reconstruct the temporal structure of the Leviton wavefunction [22].

This collection of experiments adds yet more techniques to the toolbox of the emerging field of "electronic quantum optics" [23], where quantum optics experiments are performed with electrons. Such devices could have wider applications in the field of quantum computing [24–26]. What is clear is that theoretical and numerical techniques are required to explore the inherently time-resolved nature of these experiments, as well as to propose new ones.

[3] The hole-like excitations, required to maintain charge balance, move in the opposite direction and do not enter the device proper.

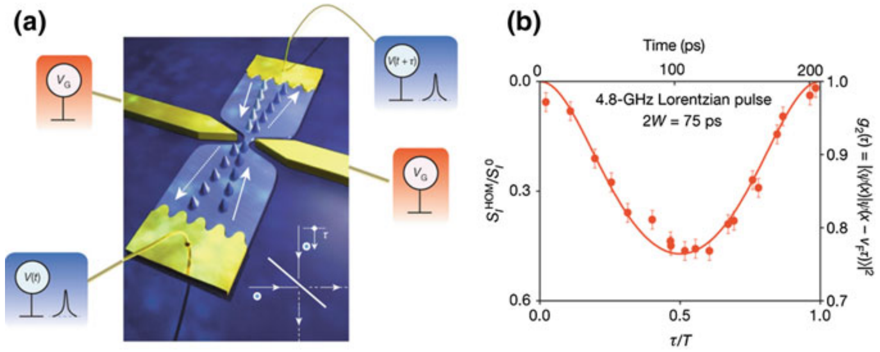

Fig. 2.4 **a** Artist's impression of a Hong-Ou-Mandel setup in a 2DEG (*dark grey*) connected via ohmic contacts (*light grey rectangles*) to metallic leads. A voltage V_g is applied to metallic gates (*light grey fingers*) to constrict the 2DEG and induce electronic backscattering. Voltage pulses $V(t)$ are applied to the leads, with a time delay τ between the pulses on the upper/lower contact. **b** Current noise measured in a single contact, as a function of the delay τ between the voltage pulses applied on each of the ohmic contacts. The noise falls to zero when there is no delay between the pulses; the fermionic nature of the single electron excitations means that each contact receives exactly one unit of charge each time a pair of electrons are injected. Figures reprinted from Ref. [19] with permission

2.3 Theoretical Description of Quantum Circuits

2.3.1 A General Model for Quantum Circuits

So now we have a bit of an idea about why it might be interesting to study time-resolved quantum transport. The next question is *how* can we study such a problem? The general class of systems that we wish to study in this thesis will consist of a number of quasi one-dimensional leads (collectively referred to as L) connected to a central device S. The basic pieces of information that we need to study such a setup are the Hamiltonian of the leads, $\hat{\mathrm{H}}^L$, the Hamiltonian of the central device, $\hat{\mathrm{H}}^S(t)$, and the lead-device coupling, $\hat{\mathrm{H}}^T(t)$. Even though there may be multiple physically separate leads, we regroup all the lead degrees of freedom into a single $\hat{\mathrm{H}}^L$. Given that we will be treating transport *through* the device, where the number of charges in the device is not fixed, it will be easiest to express the Hamiltonian using the language of second quantisation. The fundamental objects of this language are "creation" and "annihilation" operators $\hat{c}_i^\dagger$ and $\hat{c}_j$ that act on the full space of many-particle states. We aim to write expressions for observable quantities in terms of these operators, rather than in terms of the many-body wavefunctions. Although this is formally equivalent to using wavefunctions, the expressions involving the creation/annihilation operators are considerably more compact. Reference [27] contains a good introduction to this topic.

In this thesis we will not be concerned with modelling electron-electron interactions. This means that all the Hamiltonians that we will consider only contain terms that are bilinear in creation/annihilation operators (these are also referred to as "quadratic" Hamiltonians). In addition, as we will be wanting to simulate such systems on a computer, the Hamiltonians will only involve a *discrete* set of degrees of freedom (although we will be able to treat *infinite* sub-systems by exploiting translational symmetry); these are referred to as *tight-binding* models. Putting these ingredients together we can write down the most general form of Hamiltonian that we wish to treat:

$$\hat{\mathrm{H}}(t) = \underbrace{\sum_{i,j\in S} \mathrm{H}_{ij}(t)\hat{c}_i^\dagger \hat{c}_j}_{\hat{\mathrm{H}}^S(t)} + \underbrace{\sum_{i\in S,\, j\in L} \mathrm{H}_{ij}(t)\hat{c}_i^\dagger \hat{c}_j + h.c.}_{\hat{\mathrm{H}}^T(t)} + \underbrace{\sum_{i,j\in L} \mathrm{H}_{ij}\hat{c}_i^\dagger \hat{c}_j}_{\hat{\mathrm{H}}^L} . \tag{2.2}$$

The $\hat{c}_i^\dagger$ ($\hat{c}_j$) are operators that create (destroy) electrons in a single-particle state enumerated by the index i (j), which we refer to as a *site*. The site index may label position as well as other degrees of freedom such as spin or orbital angular momentum, although in specific cases we shall often make an explicit distinction between spatial and internal degrees of freedom. The $\mathrm{H}_{ij}(t)$ are time-dependent complex numbers that we collectively refer to as the matrix

$$\mathbf{H}(t) = \begin{pmatrix} \mathbf{H}^S(t) & \mathbf{H}^T(t) \\ [\mathbf{H}^T(t)]^\dagger & \mathbf{H}^L \end{pmatrix} \tag{2.3}$$

where the sub-matrices are the device ($\mathbf{H}^S$), lead ($\mathbf{H}^L$), and coupling terms ($\mathbf{H}^T$).

Given that the Hamiltonian is fully characterised by the matrix $\mathbf{H}(t)$, which is just the Hamiltonian in first quantisation, naïvely one may think that we just need to use the time-dependent Schrödinger equation on some wavepacket initial state and call it a day. The situation is, however, a little more complicated than this. The complications arise due to two aspects peculiar to *open*, *fermionic* systems. Firstly the *open* condition means that we treat the electrodes as being infinite in extent (though, for simplicity, we shall always treat them as being periodic). This has profound consequences on a mathematical level, as the spectrum of the Hamiltonian will now have a *continuous* part (that will mostly dominate the transport properties), in addition to a discrete part. Secondly, there is a filled Fermi sea already present in the system that—as we saw previously in the Hong-Ou-Mandel experiment—is crucial to obtaining the correct physics. In a system with time-dependent perturbations electrons may be excited to different energies, however the Fermi sea prevents certain transitions (to already filled states) from being possible. It is not immediately obvious how this condition can be satisfied just by solving the single-particle time-dependent Schrödinger equation. We shall see that it is the presence of the filled Fermi sea that will give us the correct initial conditions for the problem in terms of the macroscopic (and directly experimentally controllable) parameters of the system, rather than resorting to microscopic details in the form of electronic wave packets.

2.3.2 Non-equilibrium Green's Function Techniques

Historically the first class of techniques to deal with the these two issues were the non-equilibrium Green's function (NEGF) techniques. The earliest numerical simulations of time-resolved transport were based on a seminal article by Caroli et al. [28], which applied the Keldysh formalism [29] to a strictly one-dimensional (single mode) model. This technique was applied in Ref. [30] to study resonant tunneling through a device consisting of a single site. A more general formulation for generic device geometries was later proposed by Wingreen et al. [31] and Jauho et al. [32], following their own extension of the stationary non-equilibrium formalism [33], which was itself based on Ref. [28]. The formalism described in these papers is at the foundation of the non-equilibrium Green's function techniques used today.

In the NEGF approach the fundamental objects are *correlators* (called Green's functions) between the electron creation/destruction operators introduced previously. Although a whole zoo of such correlators exist, two of the most important ones are the so-called *retarded* ($\mathcal{G}^R_{ij}(t,t')$) and *lesser* ($\mathcal{G}^<_{ij}(t,t')$) Green's functions:

$$\mathcal{G}^R_{ij}(t,t') = -i\Theta(t-t')\langle\{\hat{c}^\dagger_j(t'), \hat{c}_i(t)\}\rangle \tag{2.4}$$

$$\mathcal{G}^<_{ij}(t,t') = i\langle\hat{c}^\dagger_j(t')\hat{c}_i(t)\rangle \tag{2.5}$$

where $\Theta(t-t')$ is the Heaviside function, $\{\cdot,\cdot\}$ denotes an anticommutator, the $\hat{c}^\dagger_j(t)$ and $\hat{c}_i(t)$ are creation/destruction operators in the Heisenberg picture [27]:

$$\hat{c}^\dagger_j(t) = \hat{U}(t)\,\hat{c}^\dagger_j\,\hat{U}^\dagger(t) \tag{2.6}$$

$$\hat{c}_i(t) = \hat{U}(t)\,\hat{c}_i\,\hat{U}^\dagger(t), \tag{2.7}$$

with $\hat{U}(t)$ the evolution operator satisfying $i\partial_t\hat{U}(t) = \hat{\mathrm{H}}(t)\hat{U}(t)$, and $\langle\cdot\rangle$ denotes a thermal average, i.e. $\langle\hat{A}(t)\rangle = \mathrm{Tr}\left[e^{-\hat{\mathrm{H}}(0)/k_BT}\hat{A}(t)\right]$, where $\hat{A}(t)$ is a Heisenberg-picture operator, and k_B and T are the Boltzmann constant and the temperature.[4] It turns out that all the one-body observables can be calculated from $\mathcal{G}^<_{ij}(t,t')$: for example the electron density on site i is $\rho_i(t) = -i\mathcal{G}^<_{ii}(t,t)$, and the average current between sites i and j can be written

$$I_{ij}(t) = \mathrm{H}_{ij}(t)\mathcal{G}^<_{ji}(t,t) - \mathrm{H}_{ji}(t)\mathcal{G}^<_{ij}(t,t). \tag{2.8}$$

Given that we are only interested in evaluating quantities within the device region or currents flowing between the device and the electrodes, we only need elements of

[4] This expression can be made slightly more general by replacing the operator exponential by a generic density operator, but the thermal one presented in the main text is the only one we consider in this thesis.

$\mathcal{G}^R_{ij}(t,t')$ with both indices in the device region—$i, j \in S$[5]—which we shall denote $G^R_{ij}(t,t')$ (similarly $G^<_{ij}(t,t')$ for the lesser Green's function). The equations of motion satisfied by $G^R_{ij}(t,t')$ (and its relation to $G^<_{ij}(t,t')$) can be written [27, 34]:

$$i\frac{\partial}{\partial t}\mathbf{G}^R(t,t') = \mathbf{H}^S(t)\mathbf{G}^R(t,t') + \int \mathrm{d}u\,\Sigma^R(t,u)\mathbf{G}^R(u,t'), \tag{2.9}$$

$$\mathbf{G}^<(t,t') = \int\int \mathrm{d}u\,\mathrm{d}v\,\mathbf{G}^R(t,u)\Sigma^<(u,v)\left[\mathbf{G}^R(t',v)\right]^\dagger. \tag{2.10}$$

where $\mathbf{G}^R(t,t')$ and $\mathbf{G}^<(t,t')$ are matrices with elements $G^R_{ij}(t,t')$ and $G^<_{ij}(t,t')$ respectively. The quantities $\Sigma^R(t,t')$ and $\Sigma^<(t,t')$ are the so-called retarded and lesser *self-energies* that take into account the effect of the leads, and are defined by

$$\Sigma^{R(<)}(t,t') = \mathbf{H}^T(t)\mathbf{g}^{R(<)}(t,t')\left[\mathbf{H}^T(t)\right]^\dagger, \tag{2.11}$$

where $\mathbf{g}^{R(<)}(t,t')$ is the retarded (lesser) Green's function for the leads *in isolation*, i.e. in the absence of coupling to the device region. Generally the problem to solve, therefore, takes the form of coupled integro-differential equations for several large, dense matrices.

There has been a great deal of effort over the years to design efficient strategies to integrate these equations of motion [35–39], including recursive techniques [40] and replacing the convolution-type integral with complex absorbing boundary conditions [41]. In addition the issues involved with properly including electron-electron interactions has been discussed [42–46]. Others have also derived semi-analytical expressions to calculate restricted parts of the full Green's function in specific physical situations [47–51]. An alternative but related approach introduced by Cini [52] does something a little different from the above-defined NEGF, in that one starts at $t = 0$ with the exact density matrix for the full problem and follows the system states as they are driven out of equilibrium. More recent work developed Green's function techniques within this framework [53, 54]. All these approaches are, however, fundamentally limited by the fact that the equations of motion involve dense matrices, whose number of elements scale as $\mathcal{O}(N^2)$, where N is the number of sites in the device region.

2.3.3 Wavefunction Techniques

In NEGF the Green's functions are the fundamental objects of the theory. An alternative consists in dealing directly with the many-body wavefunction of the system by

[5]We can always re-define what we consider "the device" in order to calculate currents flowing into the leads. The periodicity of the leads ensures that there will be no backscattering within the leads themselves.

calculating single-particle wavefunctions. In a non-interacting system the full many-body wavefunction is formed from a simple Slater determinant of single-particle wavefunctions, so it is at least reasonable that such an approach could be equivalent to NEGF. Nevertheless it was not clear until relatively recently [55] that there was a formal equivalence between the two approaches because of the aforementioned issues of dealing with infinite systems, as well as the Pauli principle. The use of wavefunction-based methods has recently gained popularity [56–60], with variations on the theme using a "stroboscopic" wavepacket basis [61, 62], or absorbing boundary conditions [63, 64].

In order to get a feel for how such an approach works in principle, it will be illustrative to look at a simplified example consisting of a *finite* system S at zero temperature. This will show explicitly how the Pauli principle is satisfied due to the fact that the unitary evolution of the single-particle states guarantees their mutual orthogonality at all times. We shall start with a similar model to that of Eq. (2.2), but without leads:

$$\hat{\mathrm{H}}(t) = \sum_{i,j \in S} \mathrm{H}_{ij}(t) \hat{c}_i^\dagger \hat{c}_j . \tag{2.12}$$

We shall assume that the time-dependence is only switched on for $t > 0$, so that we can diagonalise $\hat{\mathrm{H}}(t \leq 0)$:

$$\hat{\mathrm{H}}(t \leq 0) = \sum_\alpha E_\alpha \hat{d}_\alpha^\dagger \hat{d}_\alpha \tag{2.13}$$

where

$$\hat{d}_\alpha^\dagger = \sum_j [\varphi_\alpha]_j \ \hat{c}_j^\dagger \tag{2.14}$$

and the φ_α are column vectors of complex numbers (with jth element $[\varphi_\alpha]_j$) that satisfy time-independent Schrödinger equations $\mathbf{H}(t \leq 0)\varphi_\alpha = E_\alpha \phi_\alpha$. As we are at zero temperature, the full many-body state at $t \leq 0$ is just the state where all single-particle states below the Fermi energy E_F are filled:

$$|\Psi_0\rangle = \prod_{E_\alpha < E_F} \hat{d}_\alpha^\dagger |0\rangle, \tag{2.15}$$

where $|0\rangle$ is the vacuum state. The antisymmetry of $|\Psi_0\rangle$ under particle exchange is guaranteed by the anticommutation relations satisfied by the operators $\hat{d}_\alpha$:

$$\{\hat{d}_\alpha, \hat{d}_\beta\} = 0 \ , \ \{\hat{d}_\alpha, \hat{d}_\beta^\dagger\} = \delta_{\alpha\beta}, \tag{2.16}$$

where $\delta_{\alpha\beta}$ is the Kronecker delta. If we now look at times $t > 0$ the many-body state will evolve to

$$|\Psi(t)\rangle = \hat{U}(t) \prod_{E_\alpha < E_F} \hat{d}_\alpha^\dagger |0\rangle, \tag{2.17}$$

where $\hat{U}(t)$ is the evolution operator, which satisfies $i\partial_t \hat{U}(t) = \hat{\mathrm{H}}(t)\hat{U}(t)$. As $\hat{U}(t)$ is unitary, we can sandwich factors of $\hat{U}^\dagger(t)\hat{U}(t)$ between the $\hat{d}^\dagger_\alpha$'s, and use the property $\hat{U}(t)|0\rangle = |0\rangle$ to write

$$|\Psi(t)\rangle = \prod_{E_\alpha < E_F} \hat{d}^\dagger_\alpha(t)|0\rangle, \tag{2.18}$$

where $\hat{d}^\dagger_\alpha(t)$ is *defined* as

$$\hat{d}^\dagger_\alpha(t) \equiv \hat{U}(t)\,\hat{d}^\dagger_\alpha\,\hat{U}^\dagger(t). \tag{2.19}$$

Clearly the $\hat{d}^\dagger_\alpha(t)$ satisfy the equal-time anticommutation relations

$$\{\hat{d}_\alpha(t), \hat{d}_\beta(t)\} = 0\ ,\ \ \{\hat{d}_\alpha(t), \hat{d}^\dagger_\beta(t)\} = \delta_{\alpha\beta}, \tag{2.20}$$

which ensures that $|\Psi(t)\rangle$ is fully antisymmetric under particle exchange at any time t, and hence satisfies the Pauli principle at all times. We can also choose to write $\hat{d}^\dagger_\alpha(t)$ in terms of the original $\hat{c}^\dagger_j$'s

$$\hat{d}^\dagger_\alpha(t) = \sum_j \left[\psi_\alpha(t)\right]_j\ \hat{c}^\dagger_j, \tag{2.21}$$

where $\psi_\alpha(t \le 0) = \psi_\alpha$. Applying the operator $i\partial_t$ to Eqs. (2.19) and (2.21), and equating the right-hand sides, we get (after some algebra)

$$\sum_j i\left[\frac{\partial}{\partial t}\psi_\alpha(t)\right]_j \hat{c}^\dagger_j = \sum_j \sum_k \mathrm{H}_{jk}(t)\left[\psi_\alpha(t)\right]_k\ \hat{c}^\dagger_j\ , \quad \psi_\alpha(t \le 0) = \psi_\alpha. \tag{2.22}$$

As the $\hat{c}^\dagger_j$ are creation operators for *mutually orthogonal* single-particle states, we can equate the coefficients for each term j of the above sum, from which we see that $\psi_\alpha(t)$ *satisfies a time-dependent Schrödinger equation* $i\partial_t\psi_\alpha(t) = \mathbf{H}(t)\psi_\alpha(t)$. This means that in order to calculate the full many-body evolution we actually only need to solve n Schrödinger equations for all the *single-particle* states with initial energy less than the Fermi energy. Expectation values of one-body observables also take a simple form. For example, the average number of particles on site i, defined as $\langle\Psi(t)|\hat{c}^\dagger_i\hat{c}_i|\Psi(t)\rangle$ (for the zero-temperature case) can be written (after some algebra)

$$\langle\Psi(t)|\hat{c}^\dagger_i\hat{c}_i|\Psi(t)\rangle = \sum_{E_\alpha < E_F} \left|\psi_\alpha(t)\right|^2_i. \tag{2.23}$$

The expectation value of one-body operators can be written as the sum of the expectation values of the associated operators in first-quantisation, evaluated on the states with energy less than the Fermi energy. When the temperature is instead finite, the result is similar, except that the terms in the sum Eq. (2.23) are weighted by the appropriate (Fermi-Dirac) occupation factor $f(E_\alpha)$.

If we also allow the system to now contain an *infinite* number of degrees of freedom (i.e. we attach leads), the discrete energies E_α will form a continuum energy *band* and the sum Eq. (2.23) will be replaced by an integral. This last step of reasoning is not presented in a particularly rigorous way here; a proper derivation for the case of infinite systems (which also contains the case when the system starts in an out-of-equilibrium steady state) can be found in Ref. [55].

The result (in the absence of true bound states in the system) is that the thermal average of an observable $\hat{\mathrm{A}} = \Sigma_{ij} \mathrm{A}_{ij} \hat{c}_i^\dagger \hat{c}_j$ at time t can be calculated as

$$\langle \hat{\mathrm{A}}(t) \rangle = \sum_\alpha \int_{B_\alpha} \frac{\mathrm{d}E}{2\pi} \; f_\alpha(E) \psi_{\alpha E}(t)^\dagger \mathbf{A}\, \psi_{\alpha E}(t). \tag{2.24}$$

The $\psi_{\alpha E}(t)$ are time-evolved single-particle states that, at $t = 0$, were so-called *scattering states* of the system. Scattering states extend infinitely far into the leads of the system, and have the particular characteristic that their wavefunction in all of the leads is propagating *away* from the central region, except in a single lead where there is an *incoming* component (characterised by a "mode index" α). A more precise definition of scattering states is given in Chap. 3, as well as details of how to calculate them for the initial system.

The energy integral runs over the energy band B_α of the mode α: $B_\alpha = \big(\inf E_\alpha(k), \sup E_\alpha(k)\big)$ where $E_\alpha(k)$ is the dispersion relation of mode α and k runs over the Brillouin zone. $f_\alpha(E)$ is the Fermi-Dirac function associated with the lead to which the mode α belongs (different leads may have different temperatures and/or Fermi energies). We can also write the retarded and lesser Green's functions in terms of the wavefunctions [55]:

$$G^R_{ij}(t, t') = -i\Theta(t - t') \sum_\alpha \int_{B_\alpha} \frac{\mathrm{d}E}{2\pi} \; [\psi_{\alpha E}(t)]_i \left[\psi^\dagger_{\alpha E}(t')\right]_j \tag{2.25}$$

$$G^<_{ij}(t, t') = i \sum_\alpha \int_{B_\alpha} \frac{\mathrm{d}E}{2\pi} \; f_\alpha(E)\, [\psi_{\alpha E}(t)]_i \left[\psi^\dagger_{\alpha E}(t')\right]_j, \tag{2.26}$$

which forms the link between the wavefunction and Green's function based approaches.

In the next chapter we will build on the specific wavefunction method introduced in Ref. [55]. We choose to develop an entirely wavefunction based approach due to the superior scaling properties with respect to the system size and simulation time compared to direct Green's function approaches. This essentially comes down to the fact that the single-particle wavefunctions are *vectors* with N elements, as opposed to the dense matrices (N^2 elements) of the Green's function approach. This better scaling is crucial for the applications targeted in this thesis, where we study systems with a relatively large number of degrees of freedom (up to 10^4 or 10^5) in the central device region. In addition, the key role played by resonant reflection in the majority of the applications means that the dwell-time for charges in the system is also large, which necessitates long simulation times. This combination of large system size and long simulation time means that direct Green's function techniques are unsuitable. It should be noted that for other applications, such as molecular electronics, the scaling properties of the method may not be so important and a direct Green's function technique may be a better choice.

References

1. S. Datta, Electronic transport in mesoscopic systems, in *Cambridge Studies in Semiconductor Physics and Microelectronic Engineering 3* (Cambridge University Press, Cambridge, 2009)
2. R.P. Feynman et al., Quantum mechanics. Nachdr, in *The Feynman Lectures on Physics 3* (Addison-Wesley, Reading, 2007)
3. M.A. Topinka et al., Coherent branched flow in a two-dimensional electron gas. Nature **410**(6825), 183–186 (2001)
4. J.P. Bergfield, M.A. Ratner, Forty years of molecular electronics: Non-equilibrium heat and charge transport at the nanoscale: forty years of molecular electronics. Physica Status Solidi (b) **250**(11), 2249–2266 (2013)
5. M.J. Iqbal et al., Robust recipe for low-resistance ohmic contacts to a two-dimensional electron gas in a GaAs/AlGaAs heterostructure (2014). arXiv:1407.4781
6. T. Bautze et al., Theoretical, numerical, and experimental study of a flying qubit electronic interferometer. Phys. Rev. B **89**(12), 125432 (2014)
7. D. Ferry, S.M. Goodnick, *Transport in Nanostructures* (Cambridge University Press, 1997)
8. P.K. Tien, J.P. Gordon, Multiphoton process observed in the interaction of microwave fields with the tunneling between superconductor films. Phys. Rev. **129**(2), 647–651 (1963)
9. B.D. Josephson, Possible new effects in superconductive tunnelling. Phys. Lett. **1**(7), 251–253 (1962)
10. K.K. Likharev, *Dynamics of Josephson Junctions and Circuits* (Gordon and Breach Science Publishers, New York, 1986)
11. H. Pothier et al., Single-electron pump based on charging effects. EPL **17**(3), 249 (1992)
12. P.W. Brouwer, Scattering approach to parametric pumping. Phys. Rev. B **58**(16), R10135–R10138 (1998)
13. G. Fève et al., An on-demand coherent single-electron source. Science **316**(5828), 1169–1172 (2007)
14. A. Mahé et al., Current correlations of an on-demand single-electron emitter. Phys. Rev. B **82**(20) (2010)
15. F.D. Parmentier et al., Current noise spectrum of a single-particle emitter: theory and experiment. Phys. Rev. B **85**(16) (2012)
16. E. Bocquillon et al., electron quantum optics: partitioning electrons one by one. Phys. Rev. Lett. **108**(19) (2012)
17. E. Bocquillon et al., Coherence and indistinguishability of single electrons emitted by independent sources. Science **339**(6123), 1054–1057 (2013)
18. J. Dubois et al., Integer and fractional charge Lorentzian voltage pulses analyzed in the framework of photon-assisted shot noise. Phys. Rev. B **88**(8) (2013)
19. J. Dubois et al., Minimal-excitation states for electron quantum optics using levitons. Nature **502**(7473), 659–663 (2013)
20. L.S. Levitov, H. Lee, G.B. Lesovik, Electron counting statistics and coherent states of electric current. J. Math. Phys. **37**(10), 4845–4866 (1996)
21. J. Keeling, I. Klich, L.S. Levitov, Minimal excitation states of electrons in one-dimensional wires. Phys. Rev. Lett. **97**(11) (2006)
22. T. Jullien et al., Quantum tomography of an electron. Nature **514**(7524), 603–607 (2014)
23. C. Grenier et al., Electron quantum optics in quantum hall edge channels. Mod. Phys. Lett. B **25**(12n13), 1053–1073 (2011)

24. D.P. DiVincenzo, Quantum computation. Science **270**(5234), 255–261 (1995)
25. B.M. Terhal, M.M. Wolf, A.C. Doherty, Quantum entanglement: a modern perspective. Phys. Today **56**(4), 46–52 (2003)
26. C.W.J. Beenakker et al., Proposal for production and detection of entangled electron-hole pairs in a degenerate electron gas. Phys. Rev. Lett. **91**(14) (2003)
27. J. Rammer, *Quantum Field Theory of Non-equilibrium States* (Cambridge University Press, Cambridge, 2007)
28. C. Caroli et al., Direct calculation of the tunneling current. J. Phys. C Solid State Phys. **4**(8), 916–929 (1971)
29. L.V. Keldysh, Diagram technique for nonequilibrium processes. JETP **20**(47), 1515 (1964)
30. H.M. Pastawski, Classical and quantum transport from generalized Landauer-Büttiker equations. II. Time-dependent resonant tunneling. Phys. Rev. B **46**(7), 4053–4070 (1992)
31. N.S. Wingreen, A.-P. Jauho, Y. Meir, Time-dependent transport through a mesoscopic structure. Phys. Rev. B **48**(11), 8487–8490 (1993)
32. A.-P. Jauho, N.S. Wingreen, Y. Meir, Time-dependent transport in interacting and noninteracting resonant-tunneling systems. Phys. Rev. B **50**(8), 5528–5544 (1994)
33. Y. Meir, N.S. Wingreen, Landauer formula for the current through an interacting electron region. Phys. Rev. Lett. **68**(16), 2512–2515 (1992)
34. J. Rammer, H. Smith, Quantum field-theoretical methods in transport theory of metals. Rev. Mod. Phys. **58**(2), 323–359 (1986)
35. Y. Zhu et al., Time-dependent quantum transport: direct analysis in the time domain. Phys. Rev. B **71**(7), 075317 (2005)
36. C. Eduardo, Cuansing and Gengchiau Liang. J. Appl. Phys. **110**(8), 083704 (2011)
37. A. Prociuk, B.D. Dunietz, Modeling time-dependent current through electronic open channels using a mixed time-frequency solution to the electronic equations of motion. Phys. Rev. B **78**(16), 165112 (2008)
38. A. Croy, U. Saalmann, Propagation scheme for nonequilibrium dynamics of electron transport in nanoscale devices. Phys. Rev. B **80**(24), 245311 (2009)
39. V. Moldoveanu, V. Gudmundsson, A. Manolescu, Transient regime in nonlinear transport through many-level quantum dots. Phys. Rev. B **76**(8), 085330 (2007)
40. D. Hou et al., Time-dependent transport: time domain recursively solving NEGF technique. Phys. E Low-Dimension. Syst. Nanostruct. **31**(2), 191–195 (2006)
41. L. Zhang, J. Chen, J. Wang, First-principles investigation of transient current in molecular devices by using complex absorbing potentials. Phys. Rev. B **87**(20), 205401 (2013)
42. Y. Wei, J. Wang, Current conserving nonequilibrium ac transport theory. Phys. Rev. B **79**(19), 195315 (2009)
43. J. Wang, Time-dependent quantum transport theory from non-equilibrium Green's function approach. J. Comput. Electron. **12**(3), 343–355 (2013)
44. D. Kienle, M. Vaidyanathan, F. Léonard, Self-consistent ac quantum transport using nonequilibrium Green functions. Phys. Rev. B **81**(11), 115455 (2010)
45. P. Myöhänen et al., A many-body approach to quantum transport dynamics: Initial correlations and memory effects. EPL (Europhys. Lett.) **84**(6), 67001 (2008)
46. C. Verdozzi, C.-O. Almbladh, Kadanoff-Baym dynamics of Hubbard clusters: performance of many-body schemes, correlation-induced damping and multiple steady and quasi-steady states. Phys. Rev. B **82**(15), 155108 (2010)
47. J. Maciejko, J. Wang, H. Guo, Time-dependent quantum transport far from equilibrium: an exact nonlinear response theory. Phys. Rev. B **74**(8), 085324 (2006)
48. R. Tuovinen et al., Time-dependent Landauer-Büttiker formula: application to transient dynamics in graphene nanoribbons. Phys. Rev. B **89**(8), 085131 (2014)
49. M. Ridley, A. MacKinnon, L. Kantorovich, Current through a multilead nanojunction in response to an arbitrary time-dependent bias. Phys. Rev. B **91**(12), 125433 (2015)
50. M. Ridley, A. MacKinnon, L. Kantorovich, Calculation of the current response in a nanojunction for an arbitrary time-dependent bias: application to the molecular wire. J. Phys. Conf. Ser. **696**(1), 012017 (2016)

51. K.T. Cheung et al., Order O(1) algorithm for first-principles transient current through open quantum systems (2016). arXiv:1602.01638
52. M. Cini, Time-dependent approach to electron transport through junctions: general theory and simple applications. Phys. Rev. B **22**(12), 5887–5899 (1980)
53. G. Stefanucci, C.-O. Almbladh, Time-dependent partition-free approach in resonant tunneling systems. Phys. Rev. B **69**(19), 195318 (2004)
54. E. Perfetto, G. Stefanucci, M. Cini, Time-dependent transport in grapheme nanoribbons. Phys. Rev. B **82**(3), 035446 (2010)
55. Benoit Gaury et al., Numerical simulations of time-resolved quantum electronics. Phys. Rep. **534**(1), 1–37 (2014)
56. G. Stefanucci et al., Time-dependent approach to electron pumping in open quantum systems. Phys. Rev. B **77**(7), 075339 (2008)
57. S. Kurth et al., Time-dependent quantum transport: a practical scheme using density functional theory. Phys. Rev. B **72**(3), 035308 (2005)
58. G. Stefanucci, E. Perfetto, M. Cini, Ultrafast manipulation of electron spins in a double quantum dot device: a real-time numerical and analytical study. Phys. Rev. B **78**(7), 075425 (2008)
59. X. Qian et al., Time-dependent density functional theory with ultrasoft pseudopotentials: real-time electron propagation across a molecular junction. Phys. Rev. B **73**(3), 035408 (2006)
60. Z. Zhou, S.-I. Chu, A time-dependent momentum-space density functional theoretical approach for electron transport dynamics in molecular devices. EPL (Europhys. Lett.) **88**(1), 17008 (2009)
61. P. Bokes, F. Corsetti, R.W. Godby, Stroboscopic wave-packet description of nonequilibrium many-electron problems. Phys. Rev. Lett. **101**(4), 046402 (2008)
62. M. Konôpka, P. Bokes, Wave-packet representation of leads for efficient simulations of time-dependent electronic transport. Phys. Rev. B **89**(12), 125424 (2014)
63. R. Baer et al., Ab initio study of the alternating current impedance of a molecular junction. J. Chem. Phys. **120**(7), 3387–3396 (2004)
64. B. Novakovic, G. Klimeck, Atomistic quantum transport approach to time-resolved device simulations, in *2015 International Conference on Simulation of Semiconductor Processes and Devices (SISPAD)*, September 2015, pp. 8–11

http://www.springer.com/978-3-319-63690-0

Numerical Methods for Time-Resolved Quantum Nanoelectronics
Weston, J.
2017, XIII, 138 p. 53 illus., 10 illus. in color., Hardcover
ISBN: 978-3-319-63690-0